AIAA JOURNAL
Vol. 42, No. 1, January 2004

Evolution of Disturbances in Entropy Layer on Blunted Plate in Supersonic Flow

Alexander Fedorov*
Moscow Institute of Physics and Technology, 140180, Zhukovski, Moscow Region, Russia
and
Anatoli Tumin†
University of Arizona, Tucson, Arizona 85721

Linear and nonlinear stability analyses of the entropy layer over a blunted plate are discussed. Results of the linear stability theory are compared with the direct numerical solution of the Euler equations when a disturbance of prescribed frequency is imposed on the mean flow. A solver of the Euler equations based on the space–time conservation element/solution element method predicts linear and nonlinear dynamics of unstable disturbances with high accuracy. The nonlinear effect demonstrates a trend to saturation of the entropy-layer disturbances.

Nomenclature

c	=	phase speed
L	=	length of the plate
M	=	freestream Mach number
P	=	pressure
p	=	pressure disturbance
Re	=	Reynolds number
r	=	leading-edge radius
T	=	temperature
t	=	time
U, V	=	streamwise and vertical velocities
u, v	=	disturbances of streamwise and vertical velocities
x, y	=	streamwise and vertical coordinates
α	=	wave number
γ	=	specific heat ratio
δ	=	boundary-layer thickness
δ_e	=	entropy-layer thickness
ε	=	δ/L
ε_m	=	initial amplitude of mass flux disturbance, $(\rho u)'/(\rho_\infty U_\infty)$
ε_0	=	r/L
θ	=	temperature disturbance
μ	=	viscosity
ρ	=	density
ψ	=	stream function
ω	=	frequency

Subscripts

c	=	critical
i	=	imaginary
r	=	real
∞	=	freestream

Received 22 May 2002; presented as Paper 2002-2847 at the AIAA 32nd Fluid Dynamics Conference, St. Louis, MO, 24–27 June 2002; revision received 20 February 2003; accepted for publication 19 June 2003.

*Associate Professor, Faculty of Aeromechanics and Flight Techniques, Moscow Region. Member AIAA.

†Associate Professor, Department of Aerospace and Mechanical Engineering; tumin@engr.arizona.edu. Senior Member AIAA.

I. Introduction

THE laminar–turbulent transition on a hypersonic vehicle surface depends on many parameters. One of them is the leading-edge bluntness, which can affect the transition Reynolds number dramatically. Shock-tunnel experiments[1] conducted on blunted cones at the freestream Mach number $M = 5.5$ revealed that the increase of the nosetip bluntness leads to the displacement of the transition locus downstream until its maximum value. Further increase of the nosetip radius causes a reverse movement of the transition locus. Wind-tunnel experiments[2] at $M \leq 9.3$ showed that the maximum reverse displacement rapidly increases with the freestream Mach number. The transition reverse was also observed on blunted hollow cylinders and cones[3,4] at $M = 3.1$, as well as on a blunted flat plate[5] at $M = 2$. These and other data of early experiments have been summarized by Wilson.[5] Similar trends have been observed in wind-tunnel experiments[6,7] at $M = 6$ and $M = 9$. Small nosetip bluntness increases the transition Reynolds number Re_{tr}, whereas large bluntness causes a drastic reduction of Re_{tr}, relative to the sharp cone.

There were attempts to explain transition reversal on the basis of a surface roughness effect. Lysenko and Maslov[8] performed transition measurements on very cold blunted plate and concluded that ice crystals on the model surface could trip the boundary layer. Batt and Legner[9] reviewed the blunt-body experimental results emphasizing the nosetip roughness effect on transition reversal. However, much of the data did not seem to support the roughness argument.

Stability theory and experiment may help to identify the cause of the transition reverse. In a supersonic flow, the blunted leading edge of an aerodynamic body causes the formation of an upstream curved bow shock. The streamlines passing through the shock form an entropy layer of rotational inviscid flow with nonuniform velocity and temperature distributions. In turn, a viscous laminar boundary layer grows over the body surface at the bottom of the entropy layer. Interaction between mean flows of these two layers can change stability characteristics of the boundary layer and affect the transition locus.

Stability experiments[10] on slender blunted cones at $M = 8$ have provided an insight into this mechanism. For small nosetip bluntness, the boundary layer is stable to large local Reynolds numbers, and the disturbances, which enter the boundary layer, are initially attenuated. For a large bluntness, there are significant disturbances in the entropy layer above the boundary layer, and they can be several times larger than the freestream fluctuations. The entropy-layer disturbances enter the boundary layer as the entropy layer is swallowed. After entering the boundary layer, the disturbances proceed to grow rapidly at relatively small Reynolds numbers. This growth may be due to a mechanism analogous to the forcing concept described by Kendall[11] and Mack.[12] It may be that the entropy-layer disturbances are large enough to force growth of the boundary-layer disturbance and provoke early transition.

The theoretical study of Reshotko and Khan[13] and the asymptotic analysis of Sokolov[14] showed that the entropy layer on a blunt plate leads to destabilization of the second boundary-layer mode, which may be relevant to the transition reverse. Another possibility is associated with instability of the entropy layer itself. Reshotko and Khan[13] and Fedorov[15] performed linear stability analyses of the entropy layer on a blunt plate and showed that the entropy layer is inviscidly unstable due to the presence of the generalized inflection point of the mean-flow profile. However, the numerical examples in Ref. 15 indicated very small growth rates of the inviscid mode. This is consistent with hot-wire measurements, which showed very little growth of small disturbances in the entropy layer. These studies led to the conjecture that the linear growth of initially small disturbances in the entropy layer is too weak to produce disturbances of large amplitude, which could trigger a forced situation in the boundary layer.

Another scenario may be associated with bypass of the linear phase. Because freestream perturbations effectively penetrate through the bow shock, they can excite entropy-layer disturbances of relatively high initial amplitudes. Their nonlinear evolution may be essentially different from that predicted by linear stability theory. Interaction of the intensive entropy-layer disturbances with the boundary layer may also be quite different from the case of small perturbations. This motivated us to investigate linear and nonlinear dynamics of the entropy-layer disturbances. To illuminate physical aspects of the problem and minimize mathematical complexity, the body is chosen to be a flat plate with a blunt leading edge.

II. Mean Flow and Linear Stability Analysis

Consider a supersonic flow of a perfect gas over a blunted flat plate with the nose radius r as schematically shown in Fig. 1. In the nose region $\sim r$, the curved bow shock leads to formation of the entropy layer. Farther downstream, at the distance L from the leading edge, the entropy-layer thickness is of the order of $\delta_e \sim r$, whereas the laminar boundary-layer thickness is $\delta \sim \sqrt{(\mu_\infty L/\rho_\infty U_\infty)}$. In the region $1 \ll L/r \ll Re_r$ (where the nose Reynolds number $Re_r = r\rho_\infty U_\infty/\mu_\infty$ is assumed to be large), a two-dimensional weakly nonparallel rotational inviscid flow is formed in the entropy layer, whose thickness is much larger than the boundary-layer thickness. Our objective is to analyze the stability of the entropy-layer flow in this intermediate region, which is located far downstream from the leading edge and far upstream from the entropy-layer swallowing.

The longitudinal and vertical coordinates are made nondimensional as $x = x^*/r$ and $y = y^*/r$; the flow velocity components U and V, density ρ, temperature T, and pressure P are referenced to their freestream values. Following the asymptotic analyses of Yakura[16] and Van Dyke[17] (also Ref. 13), we can represent the mean-flow characteristics in the entropy layer as

$$U = U(y) + \mathcal{O}(\varepsilon_0\varepsilon) + \mathcal{O}\left(\varepsilon_0^2\right) \tag{1a}$$

$$V = \mathcal{O}(\varepsilon_0\varepsilon) + \mathcal{O}\left(\varepsilon_0^2\right) \tag{1b}$$

$$P = 1 + \mathcal{O}\left(\varepsilon_0^2\varepsilon\right) \tag{1c}$$

$$T = T(y) + \mathcal{O}(\varepsilon_0\varepsilon) + \mathcal{O}\left(\varepsilon_0^2\right) \tag{1d}$$

where $\varepsilon_0 = r/L$ and $\varepsilon = L/[r\sqrt{(L\rho_\infty U_\infty/\mu_\infty)}]$ are small parameters; $\varepsilon \sim \delta/L$. In the leading approximation, the entropy-layer profiles are expressed in the analytical form[13]

$$T(y) = \left[1 - \frac{2(M^2-1)^2}{(\gamma+1)M^2(M^2-1+\psi^2)}\right] \times \left[1 + \frac{2\gamma(M^2-1)^2}{(\gamma+1)(M^2-1+M^2\psi^2)}\right]^{1/\gamma} \tag{2}$$

$$U(y) = \left[1 - \frac{2(T-1)}{(\gamma-1)M^2}\right]^{\frac{1}{2}} \tag{3}$$

$$y = \int_0^\psi \frac{T}{U}\,\mathrm{d}\psi \tag{4}$$

Because $y^* = ry$, the entropy-layer thickness is proportional to the nose radius, whereas the nondimensional profiles $T(y)$ and $U(y)$ do not depend on the nose radius. They are functions of M and γ only.

As an example, Fig. 2 shows the temperature and velocity distributions across the entropy layer for the freestream Mach number $M = 6$ and $\gamma = 1.4$. The mean-flow temperature is highly nonuniform across the entropy layer, whereas the streamwise velocity variation is relatively small. These profiles have the generalized inflection point $y_{\text{in}} \approx 2.775$, at which $\mathrm{d}[(\mathrm{d}U/\mathrm{d}y)/T]/\mathrm{d}y = 0$, which provides a sufficient condition for the existence of unstable disturbances.[18,19]

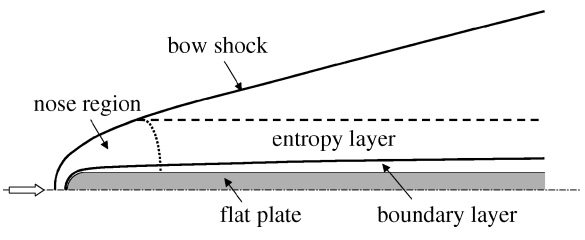

Fig. 1 Flow scheme over a blunt flat plate.

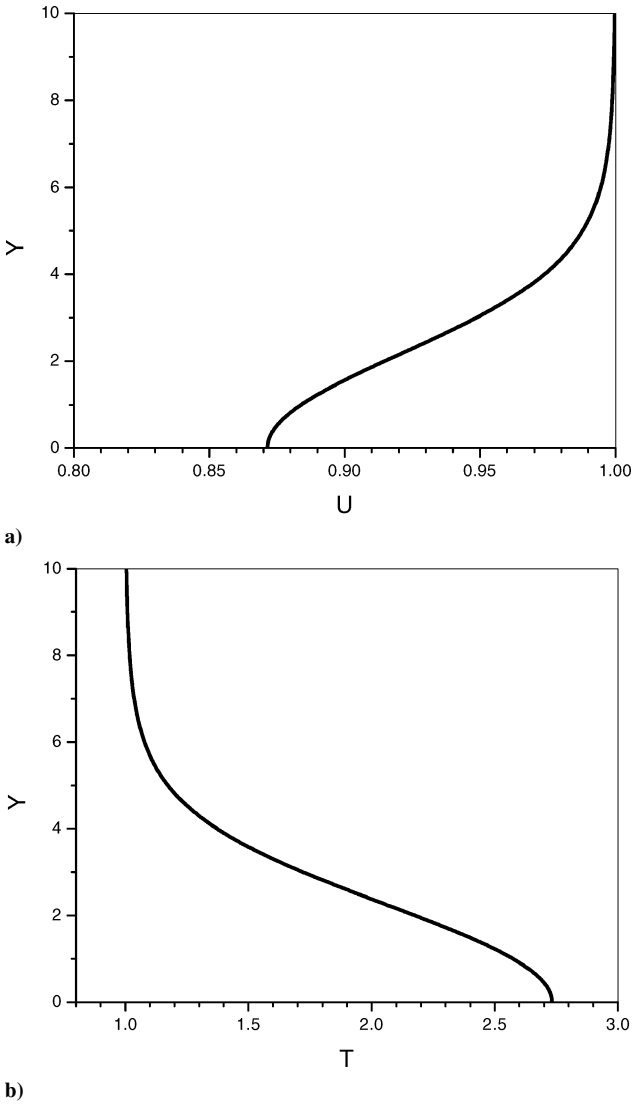

Fig. 2 Distributions across the entropy layer, $M = 6$ and $\gamma = 1.4$: a) velocity and b) temperature.

The mean flow characteristics do not depend on the longitudinal coordinate x in the region considered herein. This allows us to use stability theory for parallel flows. A two-dimensional disturbance is expressed in the elementary-wave form

$$(u', v', p', \theta') = \varepsilon_a(f, \alpha\varphi, \pi, \theta)\exp(i\alpha x - i\omega t) \tag{5}$$

where the amplitude ε_a is assumed to be small. The distributions of disturbance characteristics across the entropy layer are approximated as[15]

$$(f, \varphi, \pi, \theta) = (f_0, \varphi_0, \pi_0, \theta_0) + \mathcal{O}(\varepsilon_0\varepsilon) + \mathcal{O}(\varepsilon^2) + \mathcal{O}\left(\varepsilon_0^2\right) \tag{6}$$

In the first-order approximation, the amplitude function is a solution of the well-known ordinary differential equation (ODE) system[20] describing inviscid stability of parallel flows:

$$\frac{\mathrm{d}\varphi_0}{\mathrm{d}y} - \frac{\mathrm{d}U}{\mathrm{d}y}\frac{\varphi_0}{U-c} = -i\frac{U-c}{\gamma}\left[1 - \frac{T}{M^2(U-c)^2}\right]\pi_0 \tag{7a}$$

$$\frac{\mathrm{d}\pi_0}{\mathrm{d}y} = -i\gamma M^2\alpha^2\frac{U-c}{T}\varphi_0 \tag{7b}$$

$$(\varphi_0, \pi_0) \to 0, \qquad y \to \infty \tag{7c}$$

$$\varphi_0 = 0, \qquad y = 0 \tag{7d}$$

where the complex phase speed is $c = \omega/\alpha$.

The system (7a–7d) is integrated numerically using the fourth-order Runge–Kutta method. The integration starts in the freestream and continues to the wall. To resolve the singularity at the critical point $y_c : U(y_c) = c$, the numerical integration is carried out along a contour in the complex y plane. For unstable disturbances, the critical point is bypassed from below in the complex y plane as described in Ref. 20. With the number of grid points $N = 101$, the eigenvalue α is calculated with the accuracy $\sim 10^{-6}$. Figure 3 shows the wave number α_r and the spatial growth rate $-\alpha_i$ of the unstable entropy-layer mode as a function of the nondimensional frequency $\omega = \omega^* U_\infty/r$ for the Mach number $M = 6$. It is seen that the phase speed $c_r = \omega/\alpha_r$ is nearly constant. Its value corresponds to the critical point $y_c : U(y_c) = c_r$, which is located in the vicinity

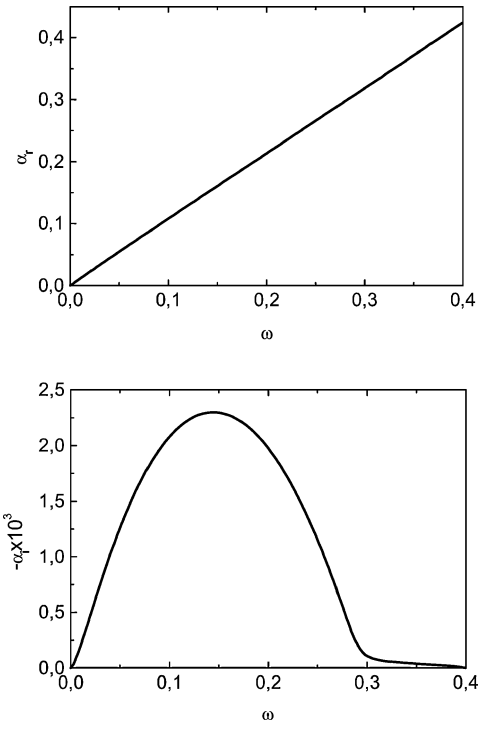

Fig. 3 Characteristics of unstable disturbance for the entropy layer: $M = 6$ and $\gamma = 1.4$.

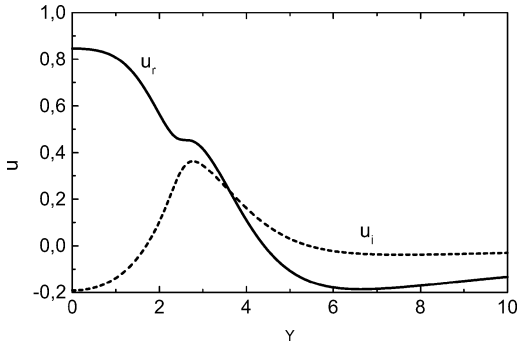

Fig. 4 Profiles of the streamwise velocity disturbance $u(y)$ for $\omega = 0.145$ and $\alpha = 0.15549 - i0.0023$: $M = 6$ and $\gamma = 1.4$.

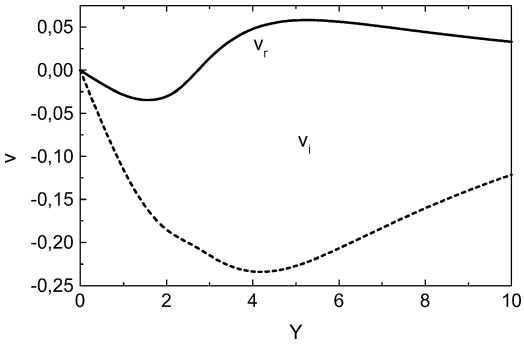

Fig. 5 Profiles of the vertical velocity disturbance $v(y)$; parameters are the same as in Fig. 3.

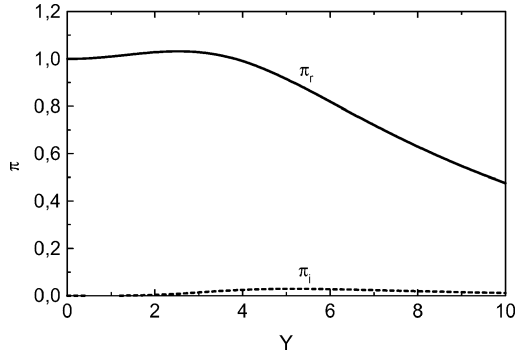

Fig. 6 Pressure disturbance profile $\pi(y)$; parameters are the same as in Fig. 3.

of the inflection point y_{in}. The disturbance growth rate is relatively small, that is, 10 times the amplification of the most unstable wave occurs on the length of the order of $10^3 r$. This is consistent with the hot-wire anemometry data,[10] showing that the mass-flow fluctuation amplitudes in the entropy layer above the boundary layer are neutrally stable or slightly unstable. Similar results were obtained in Ref. 15 for the Mach number range $1.5 < M < 6$.

The most unstable disturbance has the frequency $\omega = 0.145$ and the eigenvalue $\alpha = 0.15549 - i0.0023$. Its eigenfunctions are shown in Figs. 4–7. The temperature oscillations of the entropy-layer mode are much larger than the velocity and pressure perturbations. Maximums of the temperature and mass-flux disturbances are reached in the critical layer located near the point $y_c \approx 2.5$. The pressure and vertical velocity distributions are similar to those of the first mode calculated for a supersonic boundary layer at high Reynolds numbers.[13]

III. Conservation Element/Solution Element Euler Method

Recently, Chang et al.[21] developed a new numerical method, the space-time conservation element and solution element (CE/SE method), that allows for accurate simulation of unsteady inviscid

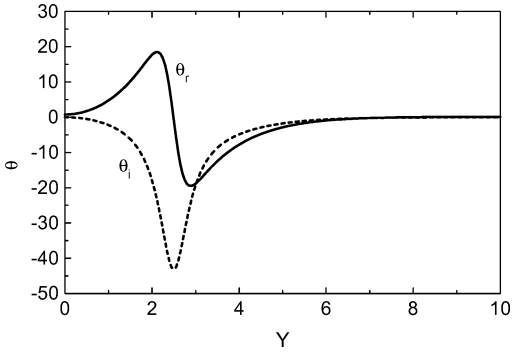

Fig. 7 Temperature disturbance profile $\theta(y)$; parameters are the same as in Fig. 3.

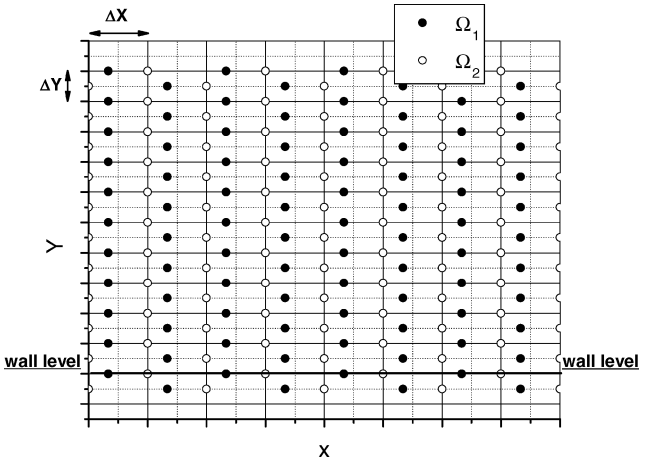

Fig. 8 Structured staggered grid.

flows including weak acoustic waves and strong shock waves. It was demonstrated[22] that the CE/SE method can be successfully used for linear and nonlinear stability analyses of compressible mixing layers. Hereafter, we apply the CE/SE method to the stability analysis of the entropy layer flow discussed in Sec. II.

We choose a rectangular computational domain in the x–y plane: $0 \le X \le 300$ and $0 \le Y \le 15$. Figure 8 shows two sets of the staggered mesh, Ω_1 and Ω_2. The first set of points (solid) corresponds to the time levels $\Delta t/2$, $3\Delta t/2$, $5\Delta t/2$, ... The second set of points (hollow) corresponds to the time levels 0, Δt, $2\Delta t$, ... Each node point of sets Ω_1 and Ω_2 has three neighbor points from the previous half-time step. The Euler equations are written as an integral conservation law in (X, Y, t) for a CE composed of the surface segments of the neighboring SEs. Interested readers are referred to Ref. 21 for details.

A uniform grid 300×150 is used with $\Delta X = 1$ and $\Delta Y = 0.1$. The initial flowfield at $M = 6$ is defined in accordance with the mean velocity and temperature profiles given by Eqs. (2) and (3). At the upper and downstream boundaries of the computation domain, we impose nonreflecting boundary conditions.[21] The boundary conditions on the wall are formulated assuming that the flowfield below the wall is the mirror image of the flow above the wall. The inflow conditions are prescribed as the mean flow plus a periodic-in-time disturbance. The dimensionless frequency is chosen to be $\omega = 0.145$, and the disturbance profiles are chosen as a solution of the linear stability equations (7) (Figs. 4–7). Afterward, the Euler equations are solved with time step $\Delta t = 0.08$.

Figure 9 shows the mass-flux disturbance field with the initial amplitude 0.565%. In these calculations, we used the CE/SE Euler method with a weighted $\alpha - \varepsilon$ scheme. (Its details are given in Ref. 21.) The weighted index $\alpha = 0$, and the parameter $\varepsilon = 0.2$, as was chosen for the analysis of the mixing layer in Ref. 22. Figure 10 shows the mass-flux amplification extracted from the numerical simulation and the linear stability theory. An exponential fit of the computation corresponds to the imaginary part $\alpha_i = -0.00236$, whereas

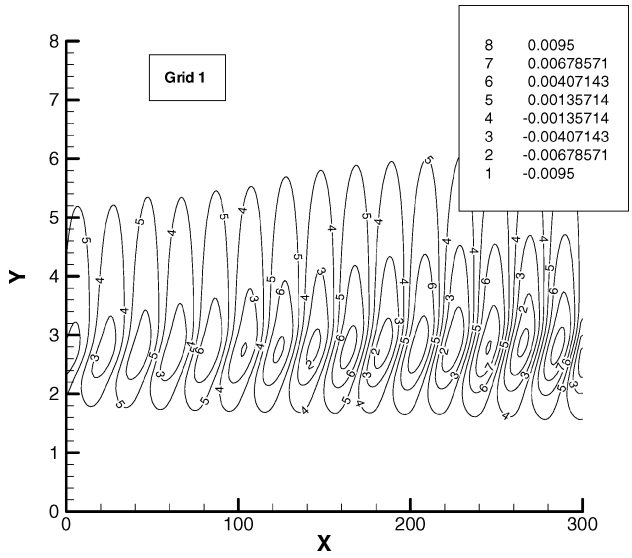

Fig. 9 Mass-flux disturbance field in the entropy layer: $M = 6$, $\omega = 0.145$, and $t = 150$.

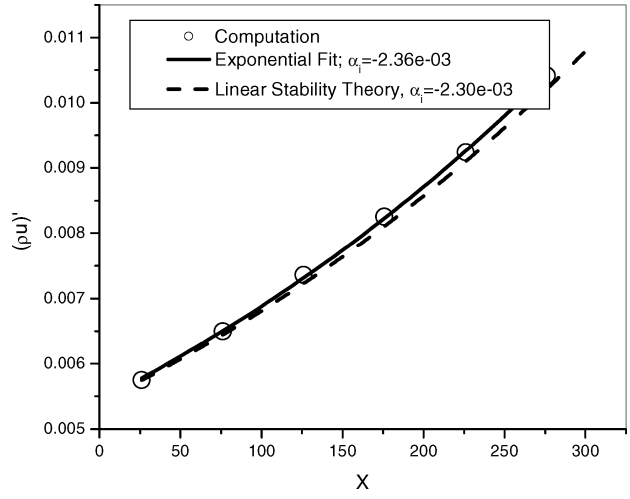

Fig. 10 Comparison of the mass-flux disturbance amplifications: $Y = 2.75$.

the linear stability theory predicts $\alpha_i = -0.00230$. Notwithstanding very small growth rates, the agreement is very good. Figure 11 shows a comparison of profiles of the mass-flux disturbance, obtained from numerical solution of the Euler equation $X = 176$ and $t = 500$, with the disturbance resulting from the linear stability analysis. The agreement between the profiles is also very good. These comparisons indicate that the CE/SE method allows for simulation of very small disturbances with very slow growth. Note that the growth rates of the mixing-layer disturbances analyzed in Ref. 22 were much higher, which was much easier for numerical simulations. Summarizing, we conclude that the CE/SE method is an effective tool for stability analysis of the entropy-layer flow.

When the initial amplitude to a parameter is changed, nonlinear dynamics of the entropy-layer disturbances can be investigated by means of direct numerical solution of the Euler equations. The nonlinear effect is demonstrated in Fig. 12 for a few initial amplitudes ε_m of the mass-flux disturbance. One can see a trend to saturation of the disturbances with the initial amplitude increase.

It is important to test the grid effect on numerical solutions for disturbances of high amplitudes. We compare the results obtained with the original grid (grid 1) and the fine grid (grid 2): $\Delta X = 0.5$, $\Delta Y = 0.05$, and $\Delta t = 0.04$. Figures 13 and 14 show the mass-flux disturbance field when the initial amplitude is 8.47%. Although the flowfields are similar, one can see their differences in the downstream region where the disturbance amplitude is approximately 10%. Figures 15 and 16 show the time signals at $X = 26$ and

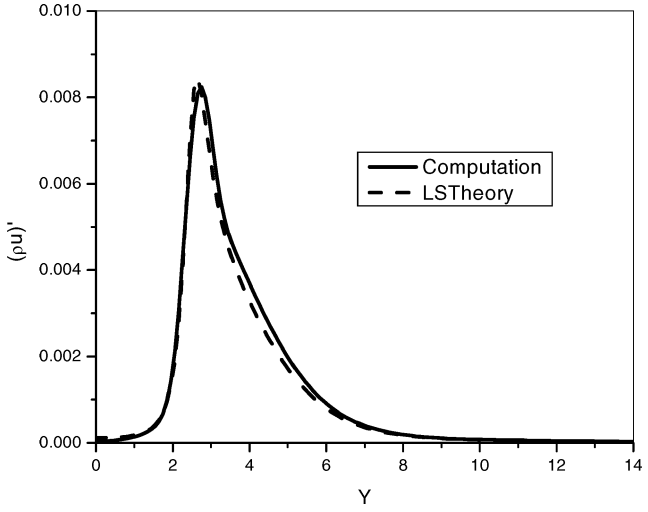

Fig. 11 Comparison of the mass-flux disturbance profiles: $X = 176$ and $t = 500$.

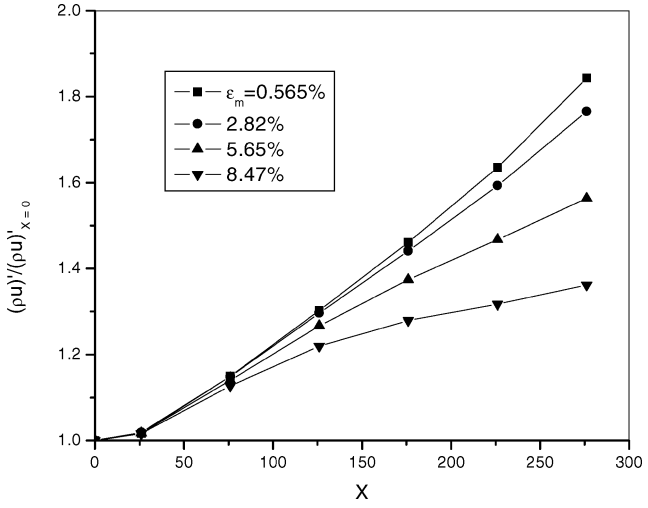

Fig. 12 Effect of the initial amplitude.

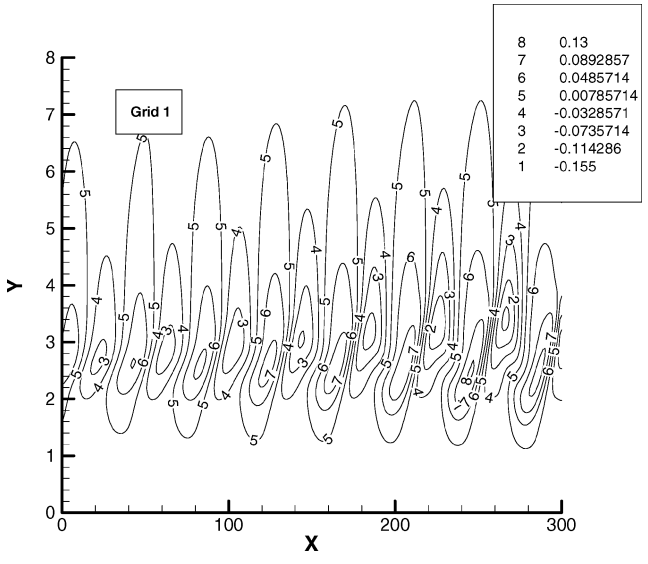

Fig. 13 Mass-flux disturbance field in the entropy layer: $\varepsilon_m = 8.47\%$ (grid 1).

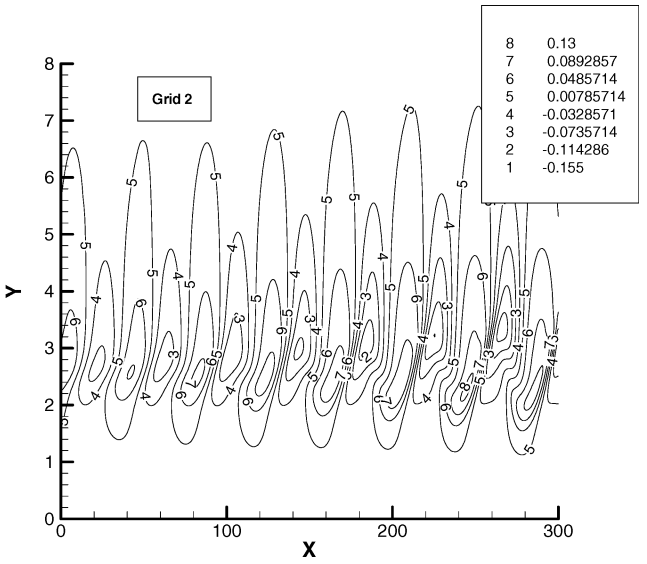

Fig. 14 Mass-flux disturbance field of in the entropy layer: $\varepsilon_m = 8.47\%$ (grid 2).

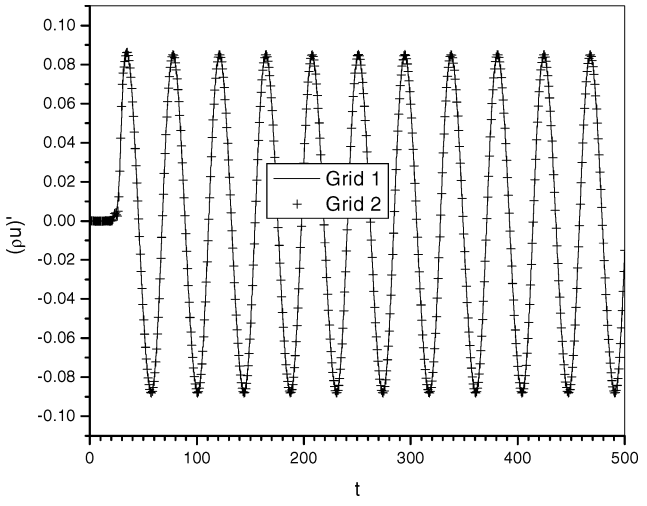

Fig. 15 Time signal: $\varepsilon_m = 8.47\%$ and $X = 26$.

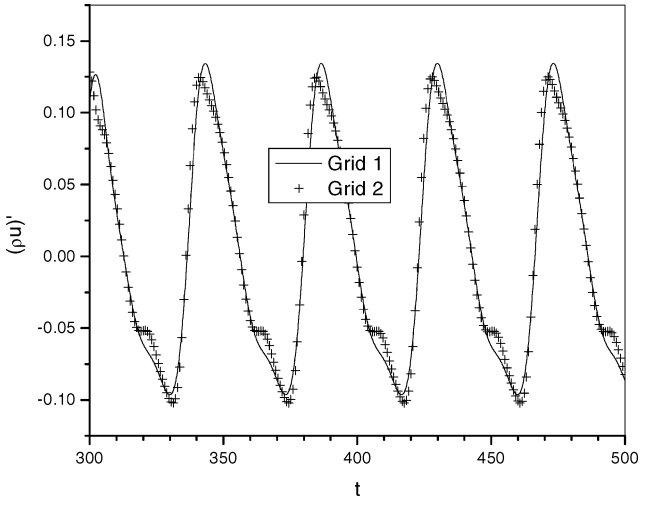

Fig. 16 Time signal: $\varepsilon_m = 8.47\%$ and $X = 276$.

$X = 276$ measured at the level $Y = 2.75$. There is no noticeable difference between these signals at $X = 26$, whereas small distortions are observed at the station $X = 276$. This indicates that one can use grid 1 for correct simulation of disturbances with mass-flux amplitudes less than 9%.

IV. Conclusions

The linear stability problem for the entropy layer over a blunted plate was analyzed using the conventional stability theory and direct numerical solution. The Euler equations were solved by the space–time CE/SE method. It was shown that the latter method provides very accurate simulations of the entropy-layer disturbances with small amplitude and slow growth. It was shown that nonlinear effects lead to a trend of disturbance saturation.

As a next step, the CE/SE method can be used for the direct numerical simulation of a very interesting case, one associated with the entropy-layer disturbance entering into the boundary layer. We believe this will help to understand the physics of the transition reverse on blunted bodies at hypersonic speeds.

Acknowledgment

We thank S. C. Chang for providing all of the necessary information regarding the conservation element/solution element Euler method.

References

[1]Stetson, K. F., and Rushton, G. H., "Shock Tunnel Investigation of Boundary Layer Transition at $M = 5.5$," *AIAA Journal*, Vol. 5, No. 5, 1967, pp. 899–906.

[2]Stetson, K. F., "Effect of Bluntness and Angle of Attack on Boundary Layer Transition on Cones and Biconic Configurations," AIAA Paper 79-0269, Jan. 1979.

[3]Brinich, P. F., "Effects of Leading-Edge Geometry on Boundary Layer Transition at Mach 3.1," NACA TN-3659, March 1956.

[4]Brinich, P. F., and Sands, N., "Effects of Bluntness on Transition for a Cone and a Hollow Cylinder at Mach 3.1," NACA TN-3679, May 1957.

[5]Wilson, R. E., "Laminar Boundary Layer Growth at Hypersonic Speeds," *Journal of Spacecraft and Rockets*, Vol. 2, 1965, pp. 490–496.

[6]Stetson, K. F., "Nosetip Bluntness Effects on Cone Frustum Boundary Layer Transition in Hypersonic Flow," AIAA Paper 83-1763, July 1983.

[7]Muir, J. R., and Truillo, A. A., "Experimental Investigation of the Effects of Nose Bluntness, Freestream Unit Reynolds Number, and Angle of Attack on Cone Boundary Layer Transition at a Mach Number of 6," AIAA Paper 72-216, Jan. 1972.

[8]Lysenko, V. I., and Maslov, A. A., "Transition Reversal and One of Its Causes," *AIAA Journal*, Vol. 19, No. 6, 1981, pp. 705–708.

[9]Batt, R. G., and Legner, H. H., "A Review of Roughness Induced Nosetip Transition," AIAA Paper 81-1223, June 1981.

[10]Stetson, K. F., and Kimmel, R. L., "On Hypersonic Boundary-Layer Stability," AIAA Paper 92-0737, Jan. 1992.

[11]Kendall, J. M., "Wind Tunnel Experiments Relating to Supersonic and Hypersonic Boundary Layer Transition," *AIAA Journal*, Vol. 13, No. 3, 1975, pp. 290–299.

[12]Mack, L. M., "Linear Stability Theory and the Problem of Supersonic Boundary-Layer Transition," *AIAA Journal*, Vol. 13, No. 3, 1975, pp. 278–289.

[13]Reshotko, E., and Khan, M. M. S., "Stability of the Laminar Boundary Layer on a Blunted Plate in Supersonic Flow," *Symposium on Laminar-Turbulent Transition*, Springer-Verlag, Berlin, 1980, pp. 186–200.

[14]Sokolov, L. A., "Influence of the Entropy Layer on the Propagation of Unsteady Perturbations in a Boundary Layer with Self-Induced Pressure," *Zhurnal Prikladnaya i Mekhanika Tekhnicheskaya Fizika (Journal of Applied Mechanics and Technical Physics)*, Vol. 25, No. 3, 1984, pp. 51–53 (in Russian).

[15]Fedorov, A. V., "Instability of the Entropy Layer on a Blunt Plate in Supersonic Flow," *Zhurnal Prikladnaya i Mekhanika Tekhnicheskaya Fizika (Journal of Applied Mechanics and Technical Physics)*, Vol. 30, No. 5, 1989, pp. 63–69.

[16]Yakura, J., "Theory of Entropy Layers and Nose Blunting in Hypersonic Flow," *Hypersonic Flow Research*, edited by F. R. Riddel, Academic Press, New York, 1962, pp. 421–461.

[17]Van Dyke, M., *Perturbation Methods in Fluid Mechanics*, Academic Press, New York, 1964.

[18]Lees, L., and Lin, C. C., "Investigation of the Instability of the Laminar Boundary Layer in a Compressible Fluid," NACA TN 1115, Washington, DC, Sept. 1946.

[19]Lin, C. C., *The Theory of Hydrodynamic Stability*, Cambridge Univ. Press, London, 1955.

[20]Mack, L. M., "Boundary-Layer Stability Theory," Pt. B, Jet Propulsion Lab., JPL Doc. 900-277, California Inst. of Technology, Pasadena, CA, May 1969.

[21]Chang, S. C., Wang, X. Y., and Chow, C. Y., "The Space–Time Conservation Element and Solution Element Method: A New High-Resolution and Genuinely Multidimensional Paradigm for Solving Conservation Laws," *Journal of Computational Physics*, Vol. 156, 1999, pp. 89–136.

[22]Loh, C. Y., Hultgren, L. S., and Chang, S.-C., "Wave Computation in Compressible Flow Using Space–Time Conservation Element and Solution Element Method," *AIAA Journal*, Vol. 39, No. 5, 2001, pp. 794–801.

G. V. Candler
Associate Editor